Enhanced Hydroacoustic Range Robustness of Three-Stage Position Filter based on Long Baseline Measurements with Unknown Wave Speed ⋆

Erlend K. Jørgensen * **Tor A. Johansen** ** **Ingrid Schjølberg** *

* *Department of Marine Technology, University of Science and Technology (NTNU), 7491 Trondheim, Norway*
** *Department of Engineering Cybernetics, University of Science and Technology (NTNU), 7491 Trondheim, Norway*

Abstract: This paper considers the problem of constructing a globally convergent position- and velocity estimator with close-to-optimal noise properties using hydroacoustic long baseline measurements. Three ways of improving the range robustness of the three stage filter for long baseline measurements with unknown wave speed are suggested. One addition is employing depth measurements in addition to pseudo-range measurements, thus increasing range noise robustness and relaxing requirements for transponder placement from not co-planar to not co-linear. Furthermore, a Kalman Filter with a linear measurement model is used, instead of a pseudo-linear time-varying measurement model and a step solving an optimization problem is also added. The proposed scheme is validated through simulation and compared to a standard Extended Kalman Filter and a perfect (non-implementable) Linearized Kalman Filter using real states as linearization point. Simulations suggest that the improved three stage filter will have similar stationary performance as the EKF while having significantly better transient performance and stability subjected to inaccurate initial estimates.

Keywords: Positioning, XKF, EKF, Filtering, UGAS, LBL

1. INTRODUCTION

Range-based positioning is used in many areas today such as for indoor positioning of sensors and vehicles, and global positioning of marine vessels. Many different methods are applied for acquiring range data. Examples include the Global Navigation Satellite System (GNSS), underwater acoustic long baseline (LBL) systems, and short-range systems such as measuring signal strength of radio signals or laser-based ranging. These methods are based on measuring the range from a unit to a known base position, and determining the position based on these measurements. However, it is often not the range itself that is measured, but other parameters relating directly to the range. This paper considers the time- of-arrival (TOA) measurement in range based positioning of underwater units. The measured TOA is modeled as a pseudo-range; a range affected by an unknown parameter. As a result the measurement equation has four unknowns (cartesian position and the unknown parameter), thus requiring at least four measured pseudo-ranges to estimate the variables.

Relating the position and unknown parameter to the pseudo-ranges is a highly nonlinear estimation problem, and a review of range-based positioning can be found in Yan et al. (2013). Globally exponentially stable (GES) filters for underwater navigation using LBL measurements are suggested in Batista (2015), Batista (2014), and a globally asymptotically stable (GAS) filter is suggested in Batista et al. (2010). Some classical approaches for underwater navigation using LBL measurements can be found in Vaganay et al. (1998), Bell et al. (1991), Alcocer et al. (2007), Kinsey and Whitcomb (2004) and Whitcomb et al. (1999).

Traditionally the unknown parameter is modeled as an additive bias to take into account system clock offset between the sender and receiver, and two main types of solutions have been suggested in this case. The first is employing the pseudo-ranges as measurement equations, and using an estimator for nonlinear systems such as the Extended Kalman Filter (EKF) where a local approximate linearization of the measurement model is applied (Alcocer et al. (2007)) or a particle filter (Ko et al. (2012)). The second type of solution is employing a globally valid non-linear transform or an optimization problem to express the measurements in a linear form with respect to the states in the filter. This is called a quasi-linear time-varying measurement model, as the equations are reformulated to fit a linear measurement model either by introducing extra states or eliminating non-linear terms. When the quasi-linear measurement model has been obtained, an estimator for linear systems can be applied, such as the Kalman Filter (KF).

⋆ This work is supported by the Center of Autonomous Marine Operations and Systems (AMOS), grant no. 223254.

However, both of these approaches have weaknesses. The estimators for the nonlinear system with pseudo-range measurements do not have proven convergence, and are often based on linearizing the nonlinear equations about the current estimate, as is done in the EKF. This makes the filter dependent on sufficiently accurate initial state estimates to achieve convergence, and can also lead to slow convergence if the initial state estimates are inaccurate. It is possible to use linear filters with proven convergence by transforming pesudo-ranges into a quasi-linear measurement model. However, the nonlinear transform is not robust towards noise in each measured pseudo-range. This can lead to amplification of noise and a bias in measurements which can decrease performance. In addition, if a KF is used it is assumed that the probability distribution of the measurements is Gaussian. Even if the noise in the pseudo-ranges is approximately Gaussian, the probability distribution of the measurements after the nonlinear transform can be far from Gaussian, which can also decrease performance.

The Three-Stage Filter (TSF) suggested by Johansen et al. (2016) is seeking to combine the best properties of the two approaches; the close-to-optimal noise properties of the first approach with the globally convergent nature of the second approach. This is done in three stages; first the measurements are run through an algebraic transform. This is then used as input for a KF with a quasi-linear measurement model. The output from this filter is used as the linearization point for a Linearized Kalman Filter (LKF) using the non-linear pseudo-range measurement equations. The third stage is similar to using an EKF, but an important difference is that the linearization points are not the state estimates of the filter itself, thus eliminating the feedback in the EKF, which can otherwise cause instability. From cascade theory the system is uniformly globally asymptotically stable (UGAS) seeing as both filters in the feed-forward structure are UGAS (Loría and Panteley (2005), Johansen and Fossen (2016b)). Simulations suggest that even though the linearization points are somewhat noisy, the stationary performance of the TSF is similar to the EKF, and has quicker convergence when initial estimates are inaccurate. Furthermore, the TSF is UGAS which is a very important property guaranteeing stability of the filter.

The general approach of using a globally convergent auxiliary state estimator for providing linearization points for a LKF is called the eXogenous Kalman Filter (XKF) and is described in detail in Johansen and Fossen (2016b). Furthermore, the relation between the TSF and the XKF is discussed in Johansen and Fossen (2016a).

In the case of underwater TOA measurements, it is valuable to take into account the fact that the acoustic wave propagation speed in water can be varying, and as a result the unknown parameter can be modeled as multiplicative instead of additive. This has been done in Stovner et al. (2016), where a TSF is formulated using a pseudo-range measurement model with a multiplicative parameter. This leads to a slightly different quasi-linear measurement model, which involves a quadratic nonlinear transformation of the pseudo-range measurement. Consequently, the measurement noise of the pseudo-ranges is amplified linearly with increased pseudo-range, which can reduce performance.

The main contributions of this paper are methods for increasing the robustness of the TSF presented in Stovner et al. (2016). The proof of concept is presented and the results are verified through simulations. Robustness to pseudo-range measurement noise is essential in for example acoustic underwater positioning where temperature layers, and salinity may introduce transmission errors. We consider here three ways of making the TSF more robust towards pseudo-range measurement noise. Firstly, as almost all underwater vehicles have a pressure-sensor that relates directly to depth, the depth measurement can be used in the measurement equations. This significantly increases robustness towards pseudo-range measurement noise, and also increases robustness regarding transponder placement in the z-direction. Secondly, as the noise in the quasi-linear measurement model increases linearly with pseudo-range due to the nonlinear transformation of the pseudo-range measurement in the $\boldsymbol{C}$-matrix, it is suggested to use a calculated algebraic solution for the position and unknown parameter as the measurement instead. This solution is available in Stovner et al. (2016) as a part of calculating the quasi-linear measurement, and leads to a linear measurement model with a covariance matrix that is more complicated, but smaller in magnitude. Thirdly, the suggested improvement is adding an extra step before the first KF by solving an optimization problem resulting in a decrease in measurement bias. The paper also contains discussion regarding measurement variance and bias for the suggested scheme.

The paper is organized as follows. Section 2 describes how the computed measurements are found from the original measurements. Section 3 gives the overall structure of the position and velocity filters. Section 4 shows simulation and results, Section 5 provides a short discussion of the problem and results and Section 6 holds the conclusion.

2. COMPUTED MEASUREMENTS

2.1 Measurement Equation

The pseudo-range measurement model is based on TOA measurements for an acoustic signal in an underwater LBL system consisting of several transponders placed in fixed, known positions on the seabottom. Following the notation in Stovner et al. (2016), the range measurement y_i is described as $y_i = c_0 t_i$ where c_0 is the assumed wave propagation speed, and t_i is the TOA for the signal. However, as the wave propagation speed can vary, the real wave propagation speed, c, is modeled as c_0 multiplied with a parameter giving $c = \sqrt{\beta} c_0$. The position of the vehicle is defined as $p^n = [\, x \;\; y \;\; z \,]^T$ and the position of transponder i is defined as $\breve{p}_i^n = [\, \breve{x}_i \;\; \breve{y}_i \;\; \breve{z}_i \,]^T$, both in the NED frame. The geometric range is defined as $\rho_i = ct_i = \|p^n - \breve{p}_i^n\|$ where $\|\cdot\|$ is the 2-norm. Also considering that the TOA measurement is subject to measurement noise it is now possible to write the pseudo-range measurement equation as

$$y_i = \frac{1}{\sqrt{\beta}} (\rho_i + \epsilon_{y,i}) \tag{1}$$

where $\epsilon_{y,i}$ is assumed to be zero-mean Gaussian white noise with variance $\sigma^2_{y,i}$.

Furthermore, in most underwater vehicles a depth measurement is available. The depth measurement is modeled as

$$z_m = z + \epsilon_z \tag{2}$$

where ϵ_z is assumed to be zero-mean Gaussian white noise with variance σ^2_z.

2.2 Algebraic Transformation

In this section it is shown how to extract computed measurements for all four unknowns in the pseudo-range measurement equation (p^n and β). This is based on the approach described in Stovner et al. (2016), and follows the same notation. As there are four unknowns, it is necessary to have at least four pseudo-range measurements available to solve the equation. However, as will be discussed in this section, when a depth measurement is available, this can be used as a value for one of the unknowns, reducing both the number of unknowns and the number of needed range measurements to three. For the algebraic transformation TOA measurement noise is neglected, leading to a computed measurement which is sub-optimal with regards to variance. This is discussed further in Section 2.3 and 2.4. Neglecting measurement noise, the following measurement can be contructed

$$y_i^2 = \frac{1}{\beta}(p^n - \breve{p}_i^n)^T(p^n - \breve{p}_i^n) \tag{3}$$

Expanding the equation, defining $\bar{p}^n = [\, x \;\; y \,]^T$ and $\mathring{p}_i^n = [\, \breve{x}_i \;\; \breve{y}_i \,]^T$ and assuming $z_m \approx z$ we get

$$\beta y_i^2 = r - 2\mathring{p}_i^{n\,T}\bar{p}^n + \|\breve{p}_i^n\| - 2\breve{z}_i z_m + z_m^2 \tag{4}$$

where we have defined the auxiliary variable $r = \bar{p}^{n\,T}\bar{p}^n$.

Defining

$$\mathbf{x} = \begin{bmatrix} x \\ y \\ \beta \end{bmatrix} \quad \mathbf{M} = \begin{bmatrix} 1 & 0 & 0 \\ 0 & 1 & 0 \\ 0 & 0 & 0 \end{bmatrix}$$

where $\mathbf{M}$ is a selection matrix, it is possible to express r in terms of $\mathbf{x}$ as

$$r = \mathbf{x}^T\mathbf{M}\mathbf{x} \tag{5}$$

Furthermore, (4) can now be written as

$$\mathbf{C}\mathbf{x} - r\mathbf{l} = \mathbf{k} \tag{6}$$

where

$$\mathbf{C} = \begin{bmatrix} 2\mathring{p}_1^{n\,T} & y_1^2 \\ \vdots & \vdots \\ 2\mathring{p}_N^{n\,T} & y_N^2 \end{bmatrix}, \; \mathbf{k} = \begin{bmatrix} \|\breve{p}_1^n\| - 2\breve{z}_1 z_m + z_m^2 \\ \vdots \\ \|\breve{p}_N^n\| - 2\breve{z}_N z_m + z_m^2 \end{bmatrix}$$

N is the number of pseudo-range measurements and $\mathbf{l} = [\, 1 \; \cdots \; 1 \,]^T$, a vector of ones with dimension N.

By viewing r as an additional unknown variable, combining (5) and (6) gives $N+1$ equations with 4 unknowns. If $\mathbf{C}$ is invertible, it is possible to write

$$\mathbf{x} = r\mathbf{C}^{-1}\mathbf{l} + \mathbf{C}^{-1}\mathbf{k} \tag{7}$$

This will be the case if $N = 3$ and $\mathbf{C}$ has full rank. However, if $N > 3$ and $\mathbf{C}$ has full rank, it is possible to use the Moore-Penrose pseudo-inverse, given by

$$\mathbf{C}^\dagger = (\mathbf{C}^T\mathbf{C})^{-1}\mathbf{C}^T \tag{8}$$

(7) can now be written

$$\mathbf{x} = r\mathbf{c} + \mathbf{w} \tag{9}$$

where $\mathbf{c} = \mathbf{C}^{-1}\mathbf{l}$ and $\mathbf{w} = \mathbf{C}^{-1}\mathbf{k}$ if $N = 3$, and $\mathbf{c} = \mathbf{C}^\dagger\mathbf{l}$ and $\mathbf{w} = \mathbf{C}^\dagger\mathbf{k}$ if $N > 3$. By inserting (9) into (5) a second order equation with respect to r is obtained. The resulting two solutions for the second order equation are given by

$$r_{1,2} = \frac{-h \pm \sqrt{h^2 - 4\mathbf{c}^T\mathbf{M}\mathbf{c} \cdot \mathbf{w}^T\mathbf{M}\mathbf{w}}}{2\mathbf{c}^T\mathbf{M}\mathbf{c}} \tag{10}$$

where $h = 2\mathbf{c}^T\mathbf{M}\mathbf{w} - 1$. Considering there will be two solutions for r, it is necessary to be able to identify which solution is the correct one. There are several ways of doing this, mostly considering external information such that β should be close to 1, or that the transponders are on the seabottom and it is impossible that the vehicle is below the tranponders.

When $N > 3$ it is possible to use (6) alone and solve the linear set of equations to get a unique solution for both $\boldsymbol{x}$ and r. However, including (5) even though it is not necessary provides extra information and increases robustness towards pseudo-range noise significantly. Therefore, combining (5) and (6) and solving this set of equations is also done when $N > 3$.

It is assumed that the correct r is available, and when inserted into (9) an algebraic solution for $\mathbf{x}$, $\hat{\mathbf{x}} = \begin{bmatrix} \hat{x} \;\; \hat{y} \;\; \hat{\beta} \end{bmatrix}^T$ is obtained, which can be used as a measurement for a filter. However, at certain limited areas, depending on transponder position, r_1 and r_2 will be similar, and finding the correct r might prove difficult. In these areas the bias and variance of the result of the algebraic transformation will also increase. The areas are easily detectable by comparing r_1 and r_2, and a way of acquiring a good estimate with respect to variance and bias also for these positions is by solving an optimization problem. This will be discussed in the following section.

2.3 Post-transform Optimization

The Moore-Penrose pseudo-inverse can be viewed as the solution for the minimization problem

$$\arg\min_{\mathbf{x}} (\mathbf{k} + r\mathbf{l} - \mathbf{C}\mathbf{x})^T(\mathbf{k} + r\mathbf{l} - \mathbf{C}\mathbf{x}) \tag{11}$$

This does not take into account that $\mathbf{C}$ contains noisy elements, which is inaccurate as the noise generated by y_i^2 can be significant, and is also increasing with range. A way of taking this noise into account is suggested in Schaffrin and Wieser (2008), in which the Errors-in-Variables model is used, given by

$$\mathbf{k} = (\mathbf{C} - \mathbf{E}_\mathbf{y}) \cdot \mathbf{x} + \mathbf{e}_\mathbf{k} \tag{12}$$

where $\mathbf{C}$ is the coefficient matrix affected by the random error matrix $\mathbf{E}_\mathbf{y}$, and $\mathbf{e}_\mathbf{k}$ is the random error in $\mathbf{k}$. This approach is mentioned in Yan et al. (2013), but avoided to due to the increased computational complexity. However, due to the significant noise in $\mathbf{C}$ appearing as a result of the multiplicative unknown parameter, it is argued that the increase in performance is worth the extra computation.

Adapted for combining (5) and (6), the optimization problem is formulated as

$$\arg\min_{\mathbf{e_y}, \mathbf{e_k} \in \mathbb{R}^\mathbb{N}} \mathbf{e_y}^T\mathbf{Q}_{ey}^{-1}\mathbf{e_y} + \mathbf{e_k}^T\mathbf{Q}_{ek}^{-1}\mathbf{e_k} \tag{13}$$

subject to

$$\mathbf{k} + \mathbf{x}^T\mathbf{M}\mathbf{x} \cdot \mathbf{l} - \mathbf{C}\mathbf{x} + \mathbf{E_y}\mathbf{x} - \mathbf{e_k} = \mathbf{0} \tag{14}$$

where $\mathbf{E_y} = [\,\mathbf{0}_{Nx2}\ \mathbf{e_y}\,]$, $\mathbf{Q}_{ey} = \text{diag}(\left[Var(y_1^2), \cdots, Var(y_N^2)\right])$ and $\mathbf{Q}_{ek} = \text{diag}(\left[Var(-2\check{z}_1 z_m + z_m^2), \cdots, Var(-2\check{z}_N z_m + z_m^2)\right])$. To decrease the dimension of the problem, it is possible to assume that the noise in $\mathbf{k}$ generated by $2\check{z}_i z_m$ is small compared to the noise generated by z_m^2 and thus reducing $\mathbf{e_k}$ to $\mathbf{l} \cdot e_k$. This assumption is valid when $\check{z}_i \ll z$ seeing as $Var(-2\check{z}_i z_m) = 4\check{z}_i^2\sigma_z^2$ and $Var(z_m^2) = 4z^2\sigma_z^2 + 2\sigma_z^4$ thus making $Var(-2\check{z}_i z_m) \ll Var(z_m^2)$ when $\check{z}_i \ll z$. Furthermore, even when this is not the case, the difference in accuracy of $\mathbf{x}$ at the minima seem to be small compared to the increased computational effort of having a full $\mathbf{e_k}$.

The optimization problem formulated in (13) is not convex due to the cross-terms in the contraints in (14). Therefore, some test to detect divergence or convergence to an incorrect local minimum must be applied. As we already have a computed measurement, a simple check that the minimum is close to the computed measurement should be sufficient. Furthermore, as it is possible to use the computed measurement as the initial point for optimization, one can assume that the starting point is close to the correct global minimum.

2.4 Noise Robustness

When measurement noise is neglected, the approach above and the approach stated in Stovner et al. (2016) are equivalent. However, this is not the case in a real scenario in which both pseudo-range measurements and the depth measurement will be affected by noise. In this subsection the robustness against noise for the two approaches will be discussed.

Performing nonlinear operations on measurements affected by noise can lead to both a bias and increased variance. Because of the non-linear transform it is difficult to get an exact expression for the expected value and covariance matrix of $\hat{\mathbf{x}}$. However, other methods exist for estimating both variance and bias. This has been discussed in Gustafsson and Hendeby (2008), where approximate transformations for nonlinear functions of stochastic variables are compared, including first- and second order Taylor-series approximations, unscented transform approximation and Monte Carlo transformation. It is stated that the Monte Carlo transformation should "in the limit compute correct moments". As there are no demands for computational time in the analysis of the two approaches, the Monte Carlo transformation is used for determining bias and variance. The first order Taylor-series approximation results in a large and complex expression for the covariance matrix, and has been used in simulation to give a first order covariance approximation. This is discussed further in Section 3.2.

Both bias and variance will be compared by running a Monte Carlo transformation with 5000 samples, $\sigma_y^2 = \sigma_z^2 = (0.2\,\text{m})^2$, constant $z = -30\,\text{m}$ and x- and y-coordinates defined by the axis in the plot. The position of the transponders is $\check{p}_1^n = [\,10\ 10\ 0\,]^T$, $\check{p}_2^n = [\,10\ -10\ -1\,]^T$, $\check{p}_3^n = [\,-10\ 10\ -2\,]^T$ and $\check{p}_4^n = [\,-10\ -10\ 0\,]^T$. For each x- and y-position a measure of the variance is given by $V = \sqrt{Var(\hat{x}) + Var(\hat{y})}$ and a measure of the bias is given by $b = \sqrt{(mean(\hat{x}) - x)^2 + (mean(\hat{y}) - y)^2}$ where $\hat{x}$ and $\hat{y}$ are the position estimates given by (9). The results are shown in Fig. 1. The current scenario suggests that both the variance and the bias is significantly lower when a measurement of z is used, as suggested in this paper. The difference is smallest in a circle around the origin with a radius of around 30 m, when the pre-filter optimization is needed, but in other areas the improvement in accuracy is significant, especially with increasing distance from the transponders.

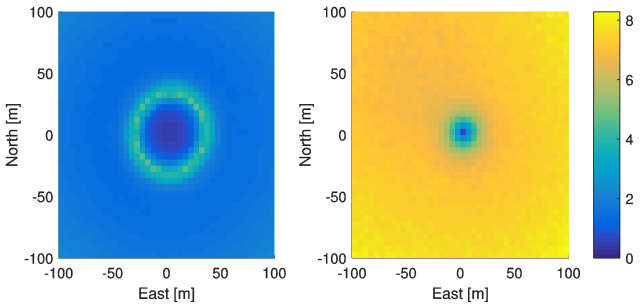

(a) Variance measure V [m]

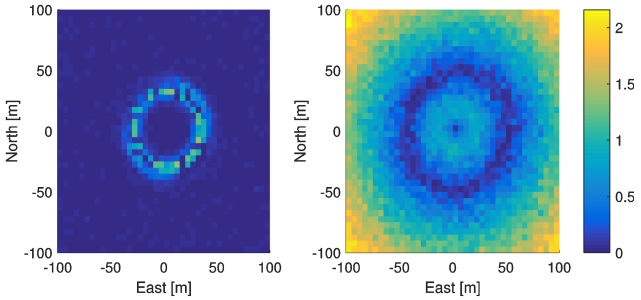

(b) Bias measure b [m]

Fig. 1. Comparison of variance and bias for computed position with and without using a depth measurement. Left plots are with depth measurement, right is without.

3. POSITION AND VELOCITY FILTERS

The overall structure of the TSF is shown in Fig. 2, and contains four subsystems which are explained in this section. The structure is similar to the structure presented in Stovner et al. (2016), with some alterations; the LTV Kalman filter in subsystem Σ_2 is exchanged with a time-invariant, linear Kalman Filter. Furthermore, the post-transform optimization is added when needed in addition to the algebraic transform in subsystem Σ_1 and the depth measurement is added to the system.

3.1 Subsystem Σ_1: Compute Measurement

The pseudo-range measurements and depth measurement are converted into measurements for p^n and β. In addition, if needed, the optimization algorithm is run. The details of this process is are discussed in Section 2.

3.2 Subsystem Σ_2: Kalman Filter

Subsystem Σ_2 is a Kalman Filter using the system model

$$\dot{p}^n = v^n$$
$$\dot{\beta} = \varepsilon_\beta$$

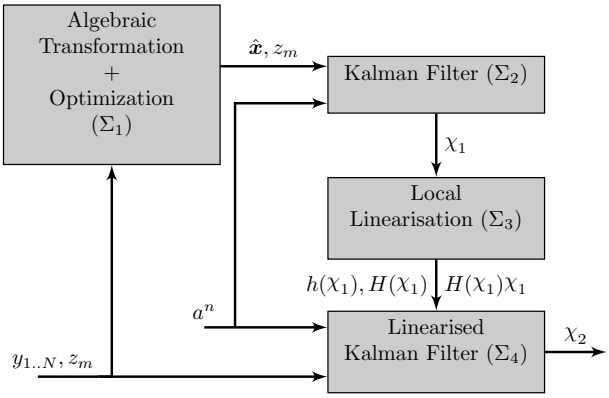

Fig. 2. Overall structure of the TSF. The three stages are Σ_1, Σ_2 and Σ_4

$$\dot{v}^n = a^n(t) + \varepsilon_a$$

or, written in matrix form

$$\dot{\chi} = \begin{bmatrix} \mathbf{0} & 0 & \mathbf{I} \\ \mathbf{0} & 0 & \mathbf{0} \\ \mathbf{0} & 0 & \mathbf{0} \end{bmatrix} \chi + \begin{bmatrix} \mathbf{0} \\ \mathbf{0} \\ \mathbf{I} \end{bmatrix} a^n(t) + \begin{bmatrix} 0 & \mathbf{0} \\ 1 & \mathbf{0} \\ 0 & \mathbf{I} \end{bmatrix} \begin{bmatrix} \varepsilon_\beta \\ \varepsilon_a \end{bmatrix} \tag{15}$$

with measurement

$$\mathbf{y} = [\, \mathbf{I}_{4x4} \;\; \mathbf{0}_{4x3} \,] \chi \tag{16}$$

where the acceleration measurement in NED frame, $a^n(t)$ is viewed as a measured input and ε_β, ε_a is the process noise with variance σ_β^2 and covariance matrix $\mathbf{R}_a$. The state estimate of this KF is denoted χ_1. It is important to note that because the acceleration measurement is in the NED frame and acceleration measurements are usually provided in the body frame, a rotation matrix relating body to NED is needed. This can be provided from an attitude and heading reference system (AHRS), such as Grip et al. (2012). The noise properties of the output from the AHRS are difficult to describe accurately due to the nonlinear filtering, thus making the choice of $\mathbf{R}_a$ non-trivial.

As discussed in Section 2.4, the covariance of the computed measurements, $\mathbf{R}_{\hat{x}}$, is dependent on σ_y^2, σ_z^2, p^n and transponder positions. This relationship is hard to find explicitly due to the nonlinear transform. However, $\mathbf{R}_{\hat{x}}$ can be approximated by employing a Taylor-series approximation. The first order Taylor-series approximation is given by (Gustafsson and Hendeby (2008))

$$\mathbf{R}_{\hat{x}} \approx \mathbf{J}\mathbf{R}_y\mathbf{J}^T \tag{17}$$

where $\mathbf{J}$ is the jacobian of $\mathbf{x}$ in (9) with respect to $\epsilon_{y,1..N}$, ϵ_z and $\mathbf{R}_y$ is the covariance matrix of $\epsilon_{y,1..N}$, ϵ_z. It is important to note that the linearization point for generating the jacobian must be chosen, either using χ_1 or $\hat{\mathbf{x}}$. $\hat{\mathbf{x}}$ is more noisy, but using χ_1 as the linearization point introduces a feedback into the system which can compromise stability. The jacobian will be approximated using finite differences, taking the central differences approach with step size h_{fd}.

3.3 Subsystem Σ_3: Local Linearization

Subsystem Σ_3 performs a first order Taylor-series linearization of the measurement equations in (1) and (2) about the state estimate generated by Σ_2, and feeds this into Σ_4. We define the measurement equation $\mathbf{h}(\chi) = [\, y_1 \; \cdots \; y_N \; z_m \,]^T$. Furthermore, we have

$$\mathbf{H}(\chi_1) = \left.\frac{\partial \mathbf{h}}{\partial \chi}\right|_{\chi=\chi_1} \tag{18}$$

The first order Taylor-series approximation about χ_1 is now given by

$$\mathbf{h}(\chi) \approx \mathbf{h}(\chi_1) + \mathbf{H}(\chi_1)(\chi - \chi_1) \tag{19}$$

$\mathbf{h}(\chi_1)$, $\mathbf{H}(\chi_1)$ and $\mathbf{H}(\chi_1)\chi_1$ are fed into Σ_4.

3.4 Subsystem Σ_4: Linearized Kalman Filter

Subsystem Σ_4 is a LKF, using the dynamic equations from (15), the measurements from (1) and (2), the measurement equation given by (19) and measurement matrix given by (18). χ_2 denotes the state estimates generated by Σ_4.

3.5 Stability Analysis

Due to the changes in the structure of the TSF, the stability proof is similar but somewhat different from Stovner et al. (2016). However, the two assumptions stated in Stovner et al. (2016) are still necessary. In addition, an assumption regarding the optimization problem, and its solution must be added:

1: The matrix $\mathbf{C}$ in (6) has full rank.

2: The ambiguity between r_1 and r_2 can be resolved.

3: The optimization problem described in Section 2.3 converges to a feasible global minimum when the estimate from (9) is used as the initial point.

It is argued in Johansen et al.Johansen and Fossen (2016b) that if Σ_2 and Σ_4 are UGAS, it follows from standard results on cascades of UGAS systems that the total system will be UGAS. This is due to the fact that the linearization point for generating the measurement matrix is being forwarded from Σ_2 and there is no feedback such that the total system is a cascade of two UGAS subsystems.

As the measurement matrix in Σ_2 given by (16) is constant, unlike in Stovner et al. (2016), the system in Σ_2 is observable regardless of the rank of $\mathbf{C}$. However, it is still necessary for $\mathbf{C}$ to have full rank as inverse/pseudo-inverse of $\mathbf{C}$ is used in the algebraic transformation and full rank is a requirement for this to exist in Σ_1. In practice this means that the transponder locations must not be colinear.

4. SIMULATION AND RESULTS

The scenario investigated in simulation is a vehicle starting at the origin, then rising 30 m before doing a lawnmower pattern lasting a total of 300 s. An example run can be seen in Fig. 3. The acceleration measurement has a frequency of 100 Hz, while the range- and depth measurements have a frequency of 1 Hz. The transponder positions are the same as in Section 2.4, $\sigma_y^2 = \sigma_z^2 = (0.2\,\text{m})^2$, $\sigma_\beta^2 = (1 \cdot 10^{-3})^2$, $\mathbf{R}_a = 0.1^2 \cdot \mathbf{I}_{3x3}$, $h_{fd} = 1 \cdot 10^{-5}$. The acceleration measurement is affected by white noise with covariance $\mathbf{R}_a$. The post-transform optimization is run if $|\hat{\beta}_1 - \hat{\beta}_2| < 0.3$ as discussed in Section 2.2.

Four different estimators will be compared by using a Monte Carlo simulation with 400 runs. Furthermore, both χ_1 and χ_2 will be plotted to show differences more detailed.

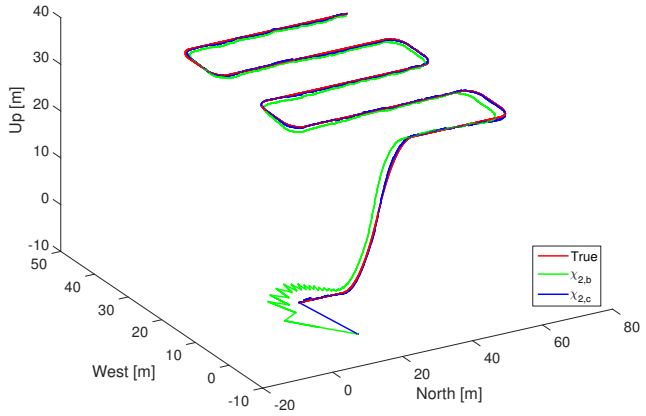

Fig. 3. Example run of simulation 2

Even though the output from the filter is Σ_4, it is of interest to see the accuracy of the linearization point output from Σ_2, χ_1. The different versions are summarized in Tab. 1. As it is argued that the TSF will have similar accuracy as the EKF, but also be globally stable, an EKF is included in the simulation. Furthermore, to give a benchmark performance, Σ_4 using true values as the linearization point is also included. Two different simulations will be performed, one with correct initial position estimate, and one with an inaccurate initial position estimate, $\hat{p}_{0,1} = [\,0\ 0\ 0\,]$, $\hat{p}_{0,2} = [\,10\ -7\ -5\,]$. $\hat{\beta}_{0,1} = 1$, $\hat{\beta}_{0,2} = 0.9$, $\hat{v} = [0,0,0]^T$, $\mathbf{Q} = diag([1 \cdot 10^{-6}, \mathbf{R}_a])$ and initial covariance matrix will be $\mathbf{P}_0 = diag([10^2, 7^2, 5^2, 0.1, 0.1, 0.1, 0.1])$ for both Σ_2 and Σ_4 in both simulations. For the EKF $\mathbf{P}_0 = diag([0.1^2, 0.1^2, 0.1^2, 0.1, 0.1, 0.1, 0.1])$ in simulation 2. This was necessary to ensure convergence.

Table 1. Filters compared in simulation

Filter	Description
a	$\sum_4$ using the exact state as linearization point
b	EKF
c	TSF
d	TSF from Stovner et al. (2016) with added depth measurement

The results are shown in Fig 4 and 5 and Tab. 2. In this scenario the performance of the TSF is very similar to the EKF when the initial position estimate is accurate, and both filters perform similar to the benchmark filter. It is apparent that the linearization point χ_1 is more noisy, with $\chi_{1,d}$ having the largest error. This is to be expected; as discussed, the algebraic transform increases noise and as shown in Section 2.4, $\chi_{1,d}$ has a larger variance and bias than $\chi_{1,c}$. In spite of this, $\chi_{2,d}$ is almost not distinguishable from $\chi_{2,a-c}$. This shows the robustness of the XKF, but it is of interest to have χ_1 as accurate as possible and in a more noisy scenario the difference in accuracy of χ_2 might increase.

When using initial estimate $p_{0,2}$ the difference between EKF and TSF is apparent; convergence of the TSF is very rapid, and much faster than the EKF due to the lack of feedback in the filter, and the fast convergence of Σ_2. The

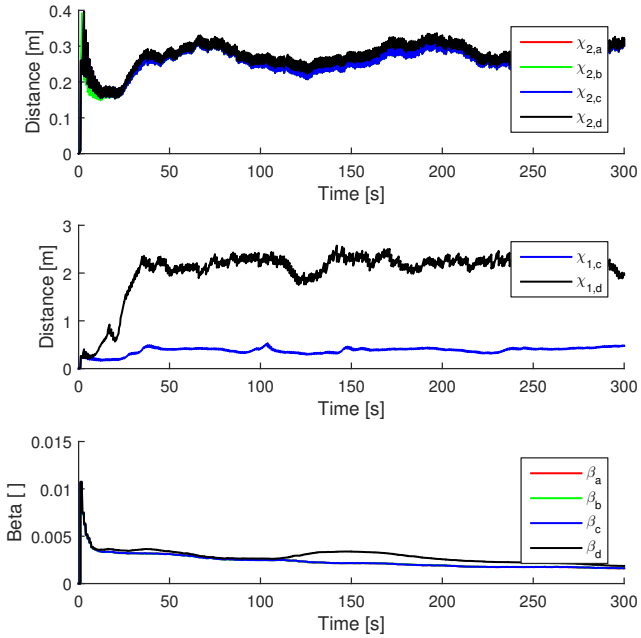

Fig. 4. RMSE for simulation 1. Euclidean distance error and error in β

EKF converges very slowly, and has a very large transient due to the necessary small $\boldsymbol{P}_0$.

In simulations performed in this section convergence of the post-transform optimization described in Section 2.3 has always been achieved, after a maximum of around 70 iterations with the SQP solver in MATLAB. Solving the optimization problem after obtaining $\hat{\mathbf{x}}$ can always be done, but simulations suggest that the improvement in accuracy seems to be worth the computational effort only when r_1 and r_2 are similar, as mentioned in Section 2.2.

5. DISCUSSION

The simulation performed in this paper shows only a very specific scenario, and it is therefore difficult to make general claims about the relative performances of the filters discussed. However, less noisy state measurements will naturally lead to more accurate estimates. As shown in Section 2.4, both variance and bias generated by pseudo-range measurement noise is reduced when a depth-measurement is added. It is important to note that the analysis is only valid for the chosen transponder setup, and setups similar to the current one.

Table 2. Mean Euclidean distance RMSE [m] over time

Filter	Simulation 1, $\hat{p}_{0,1}$	Simulation 2, $\hat{p}_{0,2}$
$\chi_{1,c}$	0.377	0.432
$\chi_{1,d}$	2.04	2.05
$\chi_{2,a}$	0.261	0.304
$\chi_{2,b}$	0.260	1.79
$\chi_{2,c}$	0.261	0.304
$\chi_{2,d}$	0.270	0.314

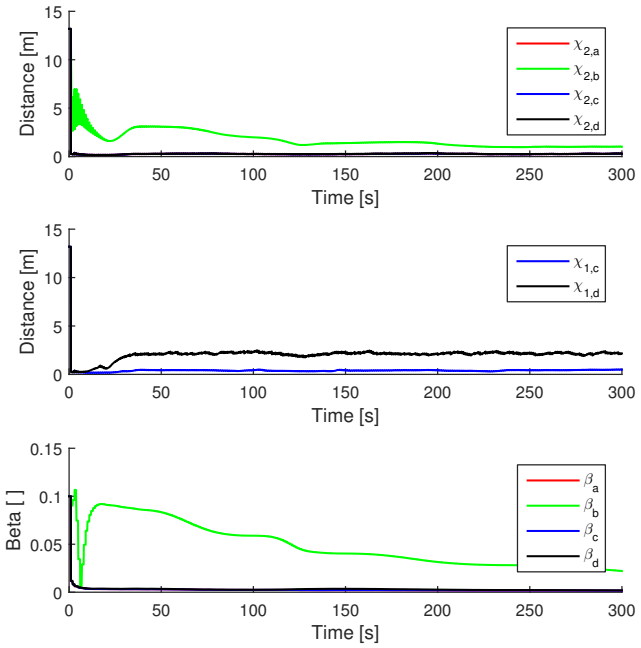

Fig. 5. RMSE for simulation 2. Euclidean distance error and error in β. The response of χ_2 from filter a,c and d is very similar, and in this plot indistinguishable

The performance of the EKF is very dependent on tuning of $\mathbf{P}_0$ and $\mathbf{Q}$. Consequently, a different tuning could have given better performance. This can also be viewed as a drawback of the EKF, and when initial estimates were inaccurate it was necessary to choose $\boldsymbol{P}_0$ far too small to ensure convergence, even though this does not reflect the real error of the initial estimate.

Assumption 3 in Section 3.5, regarding convergence of the optimization problem is an assumption that is impossible to guarantee in general due to the fact that the problem is non-convex. The optimization step is only to improve performance further, and can be omitted to have guaranteed stability properties. The need for the optimization step is dependent on the magnitude of measurement noise and transponder geometry, which must be considered for the specific scenario in which the filter is applied.

6. CONCLUSIONS

In the presented work three ways of increasing range noise robustness of the TSF in Stovner et al. (2016) has been suggested; adding a depth measurement, changing the Σ_2 measurement model and adding an optimization step when needed. This approach is compared to an EKF and a benchmark filter, an LKF using the real state as the linearization point. Simulations suggest that the stationary performance of the suggested TSF is similar to the EKF and LKF, but the transient performance of the TSF is faster when the filters have inaccurate initial state estimates. Furthermore, unlike the EKF, the TSF is UGAS, guranteeing stability.

It is important to note that no general claims about the relative performance of the suggested TSF and the EKF can be made. This is due to the fact that the performances are dependent on system configuration such as filter tuning, measurement noise and transceiver position. However, simulations suggest that ensuring convergence of the EKF may require choosing tuning parameters, especially $\mathbf{P}_0$ in an unrealistic way whereas the TSF can be tuned with realistic parameters.

REFERENCES

Alcocer, A., Oliveira, P., and Pascoal, A. (2007). Study and implementation of an EKF GIB-based underwater positioning system. *Control engineering practice*, 15(6), 689–701.

Batista, P. (2014). GES long baseline navigation with clock offset estimation. In *Control Conference (ECC), 2014 European*, 3011–3016. IEEE.

Batista, P. (2015). GES long baseline navigation with unknown sound velocity and discrete-time range measurements. *Control Systems Technology, IEEE Transactions on*, 23(1), 219–230.

Batista, P., Silvestre, C., and Oliveira, P. (2010). A sensor-based long baseline position and velocity navigation filter for underwater vehicles. *arXiv preprint arXiv:1005.4067*.

Bell, B., Howe, B., Mercer, J., and Spindel, R. (1991). Nonlinear kalman filtering of long-baseline, short-baseline, gps, and depth measurements. In *Signals, Systems and Computers, 1991. 1991 Conference Record of the Twenty-Fifth Asilomar Conference on*, 131–136. IEEE.

Grip, H.F., Fossen, T.I., Johansen, T.A., and Saberi, A. (2012). Attitude estimation using biased gyro and vector measurements with time-varying reference vectors. *Automatic Control, IEEE Transactions on*, 57(5), 1332–1338.

Gustafsson, F. and Hendeby, G. (2008). On nonlinear transformations of stochastic variables and its application to nonlinear filtering. In *Acoustics, Speech and Signal Processing, 2008. ICASSP 2008. IEEE International Conference on*, 3617–3620. IEEE.

Johansen, T.A. and Fossen, T.I. (2016a). Nonlinear filtering with eXogenous Kalman Filter and Double Kalman Filter. *European Control Conference, Aalborg, 2016*.

Johansen, T.A. and Fossen, T.I. (2016b). The eXogenous Kalman Filter (XKF). *Int. J. Control, accepted, 2016*.

Johansen, T.A., Fossen, T.I., and Goodwin, G.C. (2016). Three-stage filter for position estimation using pseudo-range measurements. *IEEE Transactions on Aerospace and Electronic Systems, accepted 2016*.

Kinsey, J.C. and Whitcomb, L.L. (2004). Preliminary field experience with the dvlnav integrated navigation system for oceanographic submersibles. *Control Engineering Practice*, 12(12), 1541–1549.

Ko, N.Y., Kim, T.G., and Moon, Y.S. (2012). Particle filter approach for localization of an underwater robot using time difference of arrival. In *OCEANS, 2012-Yeosu*, 1–7. IEEE.

Loría, A. and Panteley, E. (2005). 2 cascaded nonlinear time-varying systems: Analysis and design. In *Advanced topics in control systems theory*, 23–64. Springer.

Schaffrin, B. and Wieser, A. (2008). On weighted total least-squares adjustment for linear regression. *Journal of Geodesy*, 82(7), 415–421.

Stovner, B.B., Johansen, T.A., Fossen, T.I., and Schjølberg, I. (2016). Three-stage filter for position and velocity estimation from long baseline measurements with unknown wave speed. *American Control Conference, 2016*.

Vaganay, J., Bellingham, J.G., and Leonard, J.J. (1998). Comparison of fix computation and filtering for autonomous acoustic navigation. *International Journal of Systems Science*, 29(10), 1111–1122.

Whitcomb, L.L., Yoerger, D.R., Singh, H., and Howland, J. (1999). Combined Doppler/LBL based navigation of underwater vehicles. In *Proceedings of the the 11th International Symposium on Unmanned Untethered Submersible Technology*, 9818.

Yan, J., Tiberius, C.C., Janssen, G.J., Teunissen, P.J., and Bellusci, G. (2013). Review of range-based positioning algorithms. *IEEE Aerospace and Electronic Systems Magazine*, 28(8), 2–27.